Received: 25 August 2021 | Accepted: 9 December 2021

DOI: 10.1111/bpa.13047

Brain Pathology

RESEARCH ARTICLE

Proteomic analysis of human hippocampal subfields provides new insights into the pathogenesis of Alzheimer's disease and the role of glial cells

Yanpan Gao[1,2] | **Jiaqi Liu**[3] | **Jiayu Wang**[3,4] | **Yifan Liu**[5] | **Ling-Hui Zeng**[1] | **Wei Ge**[2,6] | **Chao Ma**[3]

[1]School of Medicine, Zhejiang University City College, Hangzhou, China

[2]State Key Laboratory of Medical Molecular Biology, Department of Immunology, Institute of Basic Medical Sciences Chinese Academy of Medical Sciences, School of Basic Medicine Peking Union Medical College, Beijing, China

[3]Department of Human Anatomy, Histology and Embryology, Neuroscience Center, National Human Brain Bank for Development and Function, Institute of Basic Medical Sciences Chinese Academy of Medical Sciences, School of Basic Medicine Peking Union Medical College, Beijing, China

[4]Department of Histology and Embryology, Basic Medical College, China Medical University, Shenyang, China

[5]Department of Neurosurgery, Peking Union Medical College Hospital, Peking Union Medical College and Chinese Academy of Medical Sciences, Beijing, China

[6]Hebei Key Laboratory of Chronic Kidney Diseases and Bone Metabolism, Affiliated Hospital of Hebei University, Baoding, China

Correspondence
Wei Ge, State Key Laboratory of Medical Molecular Biology, Department of Immunology, Institute of Basic Medical Sciences Chinese Academy of Medical Sciences, School of Basic Medicine Peking Union Medical College, No. 5 Dongdansantiao, Dongcheng District, Beijing 100005, China.
Email: wei.ge@chem.ox.ac.uk

Ling-Hui Zeng, Department of Pharmacology, School of Medicine, Zhejiang University City College, Hangzhou, Zhejiang 310015, China.
Email: zenglh@zucc.edu.cn

Chao Ma, Department of Human Anatomy, Histology and Embryology, Neuroscience Center, National Human Brain Bank for Development and Function, Institute of Basic Medical Sciences Chinese Academy of Medical Sciences, School of Basic Medicine Peking Union Medical College, No. 5 Dongdansantiao, Dongcheng District, Beijing 100005, China.
Email: machao@ibms.cams.cn

Funding information
Yanpan Gao was supported by the National Natural Science Foundation of China (81902258), the Beijing Natural Science Foundation (7192127) and the Non-profit Central Research Institute Fund of Chinese Academy of Medical Sciences (2019-RC-HL-006). Wei Ge was

Abstract

The hippocampus and entorhinal cortex (EC), the earliest affected areas, are considered relative to early memory loss in Alzheimer's disease (AD). The hippocampus is composed of heterogeneous subfields that are affected in a different order and varying degrees during AD pathogenesis. In this study, we conducted a comprehensive proteomic analysis of the hippocampal subfields and EC region in human postmortem specimens obtained from the Chinese human brain bank. Bioinformatics analysis identified region-consistent differentially expressed proteins (DEPs) which associated with astrocytes, and region-specific DEPs which associated with oligodendrocytes and the myelin sheath. Further analysis illuminated that the region-consistent DEPs functioned as connection of region-specific DEPs. Moreover, in region-consistent DEPs, the expression level of S100A10, a marker of protective astrocytes, was increased in both aging and AD patients. Immunohistochemical analysis confirmed an increase in the number of S100A10-positive astrocytes in all hippocampal subfields and the EC region of AD patients. Dual immunofluorescence results further showed that S100A10-positive astrocytes contained apoptotic neuron debris in AD patients, suggesting that S100A10-positive astrocytes may protect brain through phagocytosis of apoptotic neurons. In region-specific DEPs, the proteome showed a specific reduction of oligodendrocytes and myelin markers in CA1, CA3, and

Yanpan Gao, Jiaqi Liu, and Jiayu Wang contributed equally to this work.

supported by the National Natural Science Foundation of China (81971023). Chao Ma was supported by the CAMS Innovation Fund for Medical Sciences (CIFMS #2021-I2M-1-025)

EC regions of AD patients. Immunohistochemical analysis confirmed the loss of myelin in EC region. Above all, these results highlight the role of the glial cells in AD and provide new insights into the pathogenesis of AD and potential therapeutic strategies.

KEYWORDS
Alzheimer's disease, entorhinal cortex, glial cells, hippocampal subfields, proteomics

1 | BACKGROUND

Alzheimer's disease (AD) is a progressive neurodegenerative disease with early clinical manifestations of short-term memory loss, impaired spatial positioning, and social disorder. The middle and late stages of AD are associated with severe memory and language loss, incapacitation, and eventually death [1]. The annual incidence of AD increases dramatically with age in the United States. Previous study displayed that 0.4% developed AD in people aged 65–74, 3.2% in the age ranged from 75 to 84, and 7.6% in those aged 85 and older [2]. According to Alzheimer's Disease International, the global prevalence of dementia was approximately 50 million people worldwide in 2018, with this number predicted to triple by 2050 [3, 4].

The neuropathological hallmarks of AD include extracellular amyloid plaque (AP) depositions and intracellular neurofibrillary tangles which are composed of amyloid beta (Aβ) peptides and hyperphosphorylated tau protein, respectively [5]. The therapeutic values of Aβ and tau have been studied for almost 30 years. However, highly promising drugs targeting Aβ and tau have been recently failed to show clinical benefits in phase III trials [6, 7]. Although the US Food and Drug Administration approved Aducanumab (Biogen) for AD treatment in June 2021, there is still controversy about its therapeutic effect, because clearance of Aβ deposition by Aducanumab does not represent a clinical benefit [8].

The pathogenesis of AD is complex and remains to be fully elucidated. Previous studies have commonly focused on the alterations of neuronal cells [9, 10] and glial cells [11], displaying the activation of microglia and astrocytes, as well as the differentiation of oligodendrocytes. Glial cells account for approximately 50% of the total brain cells and play an important role in the pathogenesis of AD. Several studies showed that changes in glial cells occur earlier than the onset of neuronal death and clinical symptoms in the pathogenesis of AD, in which microglia have become a hotspot due to functions in the responses to inflammation and clearance of Aβ [12]. Although astrocytes and oligodendrocytes are also of vital importance in the pathogenesis of AD, these cell types have received relatively less attention [13–15].

The hippocampus and entorhinal cortex (EC) are the earliest and most severely affected brain regions in AD pathology. Short-term memory deficits and impaired spatial navigation in the early stage likely result from pathological changes in the hippocampus and EC [16]. The hippocampus, which plays a key role in learning and memory, consists of the cornu ammonis (CA) and dentate gyrus (DG). The CA is a heterogeneous structure divided into four histological subfields (CA1–CA4). The CA1 is usually considered to be the earliest and most severely affected subfield in AD pathology and exhibits the most significant reduction in neuron number [17], the earliest and most severe increase in Aβ deposition [18], and the most serious atrophy reflected by MRI [19, 20]. The pathology of other subfields including CA2–CA4 and DG has not yet been well clarified in AD. This probably due to the relatively small anatomical area of these subfields, which limits the accuracy of segmentation by MRI. The EC plays a pivotal role in the processing of spatial information and episodic memory. This brain region includes the lateral entorhinal cortex (LEC) and medial entorhinal cortex (MEC), and contains grid cells which are closely associated with spatial perception [21, 22]. The EC is functioned as a "gate" to transmit cortical sensory information to the hippocampus, and then back to the EC, forming the EC-hippocampal loop [23]. The signal loop between the hippocampus and MEC is of key importance in spatial perception. Therefore, a comprehensive understanding of the changes in hippocampus and EC in the pathogenesis of AD is urgently required.

Since AD was firstly defined by Alois Alzheimer in 1984, numerous studies have been performed on the pathology [24], neuroimaging [25, 26], and neural circuits [27] to clarify the pathogenesis of AD and provide new therapeutic strategies. More recently, proteomic studies have also provided helpful insights into the pathogenesis and diagnosis of AD. In these studies, diagnostic markers in blood [28, 29], cerebrospinal fluid [30], and extracellular vesicles [30–32] have been screened. Besides, disease-associated protein profiles in different regions of the brain, including the EC [33, 34], hippocampus [35–38], frontal lobe [39, 40], and temporal cortex [35, 41] have been identified. However, most of the proteomic studies of the hippocampus were reported about 10 years ago, using relatively outdated strategies that were limited by the number of identified proteins and valuable information. Additionally, proteomic analyses of the hippocampal subfields have not yet been reported.

Preclinical Alzheimer's disease (pre-AD) is the state in which AD pathology is observed while the patient's cognition is normal [42]. The ability to diagnose AD in the preclinical stage offers opportunities for early intervention. However, there is currently a lack of convenient biomarkers. Clarification of the neuroimaging, molecular, and genetic changes in the pre-AD state will provide a wealth of information that will facilitate the identification of diagnostic markers and understanding disease progression.

Thus, this study aims to investigate the protein profile changes of the hippocampal subfields of AD patients and reveals the underlying pathogenesis of AD. Postmortem brain tissues of 13 cases of AD, 9 cases of pre-AD, and 22 cases of age-matched normal donors were used. The protein profile of hippocampal subfields (CA1, CA2, CA3, and CA4/DG) and EC were identified with TMT-based quantitative proteomics and the region-specific (changed not in all brain regions) and constitute (changed in all brain regions) differentially expressed proteins were classified. Integrated proteomics, pathology, and histochemistry results highlight the role of glial cells in AD pathogenesis.

2 | METHODS

2.1 | Brain tissues and case classification

The human postmortem brain tissue samples (hippocampus and EC) used in this study were acquired from the Chinese National Human Brain Bank for Development and Function. The tissues were obtained using the standardized operational protocol for human brain banking [43]. The ECog Insider Questionnaire was used to determine clinical cognitive status [44]. For neuropathological analysis, the "ABC" dementia score for each case was used according to the National Institute on Aging and Alzheimer's Association (NIA-AA) guidelines [45]. According to the ABC and ECog score, the 44 enrolled donors were divided into three groups: normal (22 donors), pre-AD (9 donors), and AD (13 donors). The following grouping criteria were applied: normal, ABC score N or L, and ECog = 1; pre-AD, ABC score I or H, and ECog = 1; AD, ABC score I or H, and ECog > 1. All case metadata, including age, sex, disease status, ECog score, ABC score, post-mortem interval, co-existing pathology, and application, are provided in Table S1. This study was approved by the ethics committee of The Institute of Basic Medical Sciences of the Chinese Academy of Medical Sciences (Approval Number: 009-2014).

2.2 | Hippocampal dissections

The hippocampus is coronally cut into 12 pieces of equal thickness, and numbered 1–12 sequentially from the head to the tail of the hippocampus. The slice No.7 was dissected for proteomics study as previously described [46, 47]. Frozen slice No.7 was alternately sectioned into 1-mm and 30-μm sections. The 30-μm sections was fixed and then subjected to Nissl staining to determine CA1, CA2, CA3, CA4, DG, and EC regions. According to the results of Nissl staining, the subfields in the 1-mm sections were cut and separated under a microscopic dissecting microscope. Since CA4 and DG cannot be separated accurately, we put the CA4 and DG tissues together and obtained CA4/DG sample. The CA4/DG includes pyramidal layer, polymorphic layer, and granular layer enclosed in the dentate gyrus.

2.3 | Reagents and antibodies

Iodoacetamide (IAA, I2273), dithiothreitol (DTT, D9163), and urea were purchased from Sigma–Aldrich (Burlington, VT, USA). Proteinase inhibitor cocktail and sequencing-grade trypsin/Lys-C (V5071) were purchased from Promega (Madison, WI, USA). The TMT 10-plex™ and 6-plex™ Isobaric Label Reagent Sets (90110, 90061) were purchased from Thermo Fisher Scientific (Waltham, MA, USA). Anti-S100A10 (ab76472, 1:200 for IHC), anti-GFAP (ab4648, 1:400 for IF), anti-NeuN (ab104224, 1: 400 for IF) were obtained from Abcam (Cambridge, UK). Anti-MBP (HPA049222, 1:2500 for IHC) and anti-CNP (HPA023280, 1:1000 for IHC) were purchased from Sigma–Aldrich. Anti-S100A10 (S2664, 1:400 for IF), Anti-APP (mab348, 1:400 for IF) were purchased from Merck Millipore (MA). Anti-β-amyloid, 1–16 antibody (6E10 clone, SIG-39300, 1:400 for IF) was purchased from BioLegend (San Diego, CA, USA). Secondary antibodies [goat anti-mouse Alexa Fluor Plus 555 (A32727, 1:400 for IF) and goat anti-rabbit Alexa Fluor 488 (A11034, 1:400 for IF)] were obtained from Thermo Fisher Scientific (Waltham, MA, USA). Anti-rabbit HRP-DAB Two Step IHC Detection Kit (PV-9001) was purchased from ZSGB-BIO (Beijing, China). The detailed antibody information including Compony/Cat. No., Lot No., Source, Immunogen, Epitope, Application, and Reference is shown in Table S2.

2.4 | Protein sample preparation

The hippocampal tissue was homogenized by cryogenic grinding with a mortar and pestle. Tissue proteins were released using protein lysis and extraction buffer (8 M urea in PBS, pH 8.0, with proteinase inhibitors) and sonication to improve protein extraction efficiency. Soluble proteins were obtained by centrifugation at 12,000 rpm for 15 min at 4 ℃. Protein concentration was determined using a Nanodrop 2000 (Thermo Fisher Scientific).

For mass spectrometry, eight donors were divided into two groups: normal (4 cases) and AD pathology

(1 case of pre-AD and 3 cases of AD). The CA1, CA2, CA3, CA4/DG, and EC regions were included for each donor. Thus, 10 groups of samples were included in this study: CA1_Nor, CA2_Nor, CA3_Nor, CA4/DG_Nor, EC_Nor, CA1_AD, CA2_AD, CA3_AD, CA4/DG_AD, and EC_AD. Equal mass proteins of four donors in each group (25 mg each donor, total 100 mg) were pooled for digestion and mass spectrum analysis.

2.5 | Protein digestion and TMT-labeling

Proteins were treated with 10 mM DTT for 30 min followed by 25 mM IAA in the dark for 30 min at room temperature. After dilution with phosphate-buffered saline (PBS), trypsin/Lys-C was added for protein digestion. After incubation overnight, the digested peptides were heated at 60℃ for 30 min to inactivate enzyme activity, and the solution was acidified to pH 1–2 with trifluoroacetate. The digested peptides were then desalted by reverse-phase column chromatography (Oasis HLB, WAT094225, Waters) and dried with a SpeedVac vacuum concentrator. The peptide powder was dissolved in 100 µl 200 mM triethylammonium bicarbonate buffer (TEAB, pH 8.5) for Tandem Mass Tag (TMT) labeling.

TMT reagent was added to the peptide solution and incubated for 1 h at room temperature then the reaction was terminated by the addition of 5% hydroxylamine for 15 min. Three sets of TMT-labeling were conducted: Set 1 (10-plex): CA1_Nor (TMT-129C), CA2_Nor (TMT-129N), CA3_Nor (TMT-130C), CA4/DG_Nor (TMT-130N), EC_Nor (TMT-131), CA1_AD (TMT-126), CA2_AD (TMT-127N), CA3_AD (TMT-127C), CA4/DG_AD (TMT-128N), and EC_AD (TMT-128C). Set 2 (6-plex): CA1_Nor (TMT-126), CA2_Nor (TMT-127), CA3_Nor (TMT-128), CA1_AD (TMT-129), CA2_AD (TMT-130), and CA3_AD (TMT-131). Set 3 (6-plex): CA1_Nor (TMT-126), CA4/DG_Nor (TMT-127), EC_Nor (TMT-128), CA1_AD (TMT-129), CA4/DG_AD (TMT-130), and EC_AD (TMT-131). The labeled peptides in each set were then mixed, desalted, dried as described previously, and finally dissolved in 100 µl of 0.1% formic acid for high-performance liquid chromatography (HPLC) fractionation.

2.6 | HPLC fractionation and liquid chromatography (LC)-MS/MS

The peptide solution (100 µl) was transferred to a tube and loaded onto the HPLC system (UltiMate™ 3000, Thermo Fisher Scientific) equipped with an Xbridge BEH300 C18 column (1.0 ml/min, 4.6 × 250 mm, 2.5 mm, Waters). Gradient elution was performed using an alkaline eluent buffer (pH 10) consisting of phase A (5% acetonitrile in ddH_2O) and phase C (98% acetonitrile in ddH_2O). The peptides were eluted at a flow rate of 1.0 ml/min for 75 min. Fractions were collected every 90 s (50 tubes), dried and then combined into 20 tubes according to absorption peak detected at 214 nm. The peptides were then dissolved with 20 µl 0.1% formic acid for further LC-MS/MS analysis using the Orbitrap Fusion™ and Orbitrap Fusion™ Lumos™ mass spectrometers (Thermo Fisher Scientific). The two 6-plex-labeled sets were analyzed with the Orbitrap Fusion™ system and the 10-plex-labeled set was analyzed with the Fusion™ Lumos™ system. The labeled peptides were loaded into EASY-nLC 1000 system equipped with a homemade fused silica capillary column (75 µm ID, 150 mm length; Upchurch, Oak Harbor, WA, USA) packed with C-18 resin (300 A, 5 µm; Varian, Lexington, MA, USA) and separated using a 120-min gradient elution at a flow rate of 0.30 ml/min. The flowthrough peptides were ionized with the mass spectrometer in a positive-ion mode. The spectrum was collected with Xcalibur 3.0 software (Thermo Fisher Scientific) using a data-dependent acquisition model. A single full-scan mass spectrum in Orbitrap (350–1550 m/z, 120,000 resolution) was carried out, followed by a 3 s data-dependent MS/MS scan in an ion routing multipole at 38% normalized collision energy (Higher-energy collisional dissociation, HCD).

The mass spectrometry proteomics data have been deposited to the ProteomeXchange Consortium (http://proteomecentral.proteomexchange.org) via the iProX partner repository [48] with the dataset identifier PXD027380.

2.7 | Protein identification and quantification

The mass spectrum data were extracted and searched against the reviewed human protein FASTA database downloaded from UniProt (released on July 9, 2020) using Proteome Discoverer 2.2 (Thermo Fisher Scientific). The search was completed using the SEQUEST-HT algorithm according to the following criteria: a maximum of two missed cleavages allowed; precursor mass tolerance and fragment mass tolerance set at 20 ppm and 0.02 Da, respectively; total intensity threshold and minimum peak count set at 20,000 and 200, respectively; static modifications include carbamidomethylation on C and TMT 6-plex or 10-plex on the peptide N terminal; dynamic modifications include TMT 6-plex or 10-plex on K, oxidation on M, phosphate on S, T, Y and deamination on N; protein identification was considered valid when at least one peptide was detected with a false discovery rate (FDR) of less than 1%. All other parameters were set as default.

Peptides were quantified according to the unique peptide's ratio based on the TMT signals detected by MS/MS. The quantification was considered reliable with protein scores >10 and unique peptide >1. The differential expression threshold was defined with the 95% prediction interval value. The $\log_2$(ratio) ≥0.42 or ≤−0.58 was set as the differential expression threshold for 6-plex-labeling,

while $\log_2$(ratio) ≥0.32 or ≤−0.32 was set as the differential expression threshold for 10-plex-labeling (Figure S1).

2.8 | Bioinformatics analysis

Correlation and heatmap two-way cluster analysis were performed with JMP Pro 13. The correlation analysis was based on scaled protein abundance, and the heatmap was constructed using the relative AD/normal protein expression ratio. Gene ontology analysis was conducted according to PANTHER overrepresentation test (Released 20200728). The top six items filtered with gene count and fold enrichment are shown in figures. Fold enrichment is a parameter in Gene ontology enrichment analysis. It refers to the ratio of the frequency of a group of genes in a GO term to the frequency of all genes in the species in this GO term. The protein–protein interaction network was predicted with STRING (http://string-db.org) and visualized using Cytoscape 3.8.2.

2.9 | Immunohistochemical analysis

Paraffin sections of human brain tissue (each containing both hippocampus and EC region) were immersed in PBS after gradient deparaffinization and transferred to 0.01 M citrate buffer (pH 6.0) for antigen repair using the microwave method (92–98℃ for 10 min). After cooling to room temperature, sections were washed with PBS and blocked with 3% H_2O_2 for 15 min in a humid environment. Tissues were permeabilized for better antigen-antibody recognition using 0.3% Triton X-100. Sections were then blocked with 10% goat serum + 1% BSA in PBS for 30 min and incubated with primary detection antibody overnight at 4℃. Subsequently, the anti-rabbit horseradish peroxidase-diaminobenzidine (HRP-DAB) Two Step IHC Detection Kit was used for signal amplification. Sections were gradient dehydrated and sealed with a neutral resin before capturing with an Olympus BX61 microscope. Brightfield images (100× and 200× magnification) were captured (5–7 for CA1 and EC, 2 for CA4/DG, and 1 for CA2 and CA3). The brown-colored positive signal was quantified using Image-Pro Plus 6.0 software.

2.10 | Immunofluorescence analysis

Tissue deparaffinization was performed as previously described in the immunohistochemical analysis. After immersion in PBS, the tissue was permeabilized with 0.3% Triton X-100 for 30 min followed by antigen retrieval in citrate buffer using the microwave method. After neutralizing the aldehyde group with 0.5% sodium borohydride, sections were blocked and incubated sequentially with primary and secondary detection antibodies. After immersion in 70% ethanol for 2 min, sections were incubated in 0.1% Sudan Black for 10 min in the dark. Excess Sudan Black was removed by rinsing with 70% alcohol before the addition of mounting media with DAPI. The fluorescence signal was detected with an Olympus BX61 microscope equipped with a with a monochrome camera to capture fluorescent images with standard wavelength filters.

2.11 | Statistical analysis

The protein expression level in IHC was measured as mean integrated optical density (mean IOD) quantified by Image-Pro Plus 6.0. The cell number was counted in each picture and then normalized with area (per mm^2). Data were presented as the mean ± standard deviation and One-way ANOVA followed by the Bonferroni post hoc test was used to compare differences among three groups and more. $p < 0.05$ was considered to indicate statistical significance.

3 | RESULTS

3.1 | Project design

A flowchart of the study design is shown in Figure 1. We conducted a TMT-based quantitative proteomics analysis of the hippocampal subfields (CA1–CA4/DG) and EC in postmortem specimens. Bioinformatic analysis was then conducted and followed with IHC and IF verification.

In the proteomics study, eight cases were involved and divided into two groups: four donors with AD pathology (mean age 93.5 ± 7.7 y; 2 male; 3 AD and 1 pre-AD) vs. four normal donors (mean age 86.0 ± 7.3, 2 male). Two technical replicates were included for each specimen, resulting in three sets of data: one 10-plex labeled and two 6-plex labeled. Details of TMT-labeling are shown in Figure 1. For IHC analysis, forty-four cases were used to confirm myelin sheath loss and S100A10-positive astrocytes alteration in AD, including 22 cases normal, nine cases Pre-AD, and 13 cases AD. In the IF study, 17 cases were used to evaluate the function of S100A10-positive astrocytes in neuron protection, including 10 donors with AD pathology (6 AD and 4 pre-AD) and 7 normal donors. The donor's information and experimental usage of their tissues are shown in the Table S1.

3.2 | Proteomic characterization of the hippocampus and EC

Three sets of proteomics data were obtained from five brain regions: EC and hippocampus subfields CA1, CA2, CA3, CA4/DG. Set 1 (10-plex labeled) included the five regions in AD and age-matched normal donors. Set 2 and

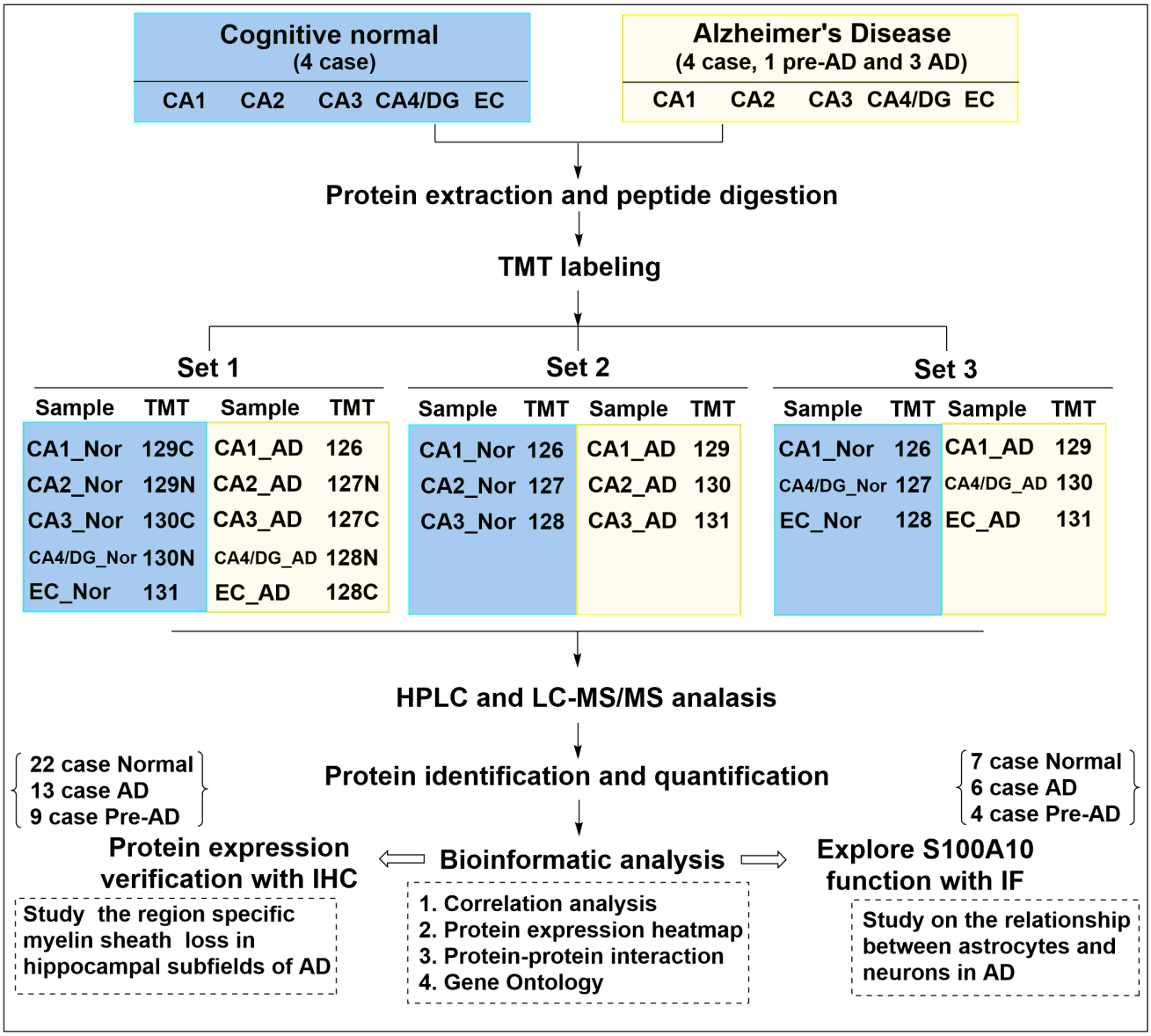

FIGURE 1 Flowchart of the study design

Set 3 (6-plex labeled) comprised duplicates of Set 1. Set 2 included CA1–CA3, and Set 3 included CA1, CA4/DG, and EC. Details of the TMT-labeling are shown in Figure 1. In total, 5389, 4579, and 4547 proteins were identified in Sets 1, 2, and 3, respectively. Of these proteins, 4133 overlapped all three sets (Figure 2A, Table S3); these proteins formed the basis of our analysis. According to the report by Zhang et al. [49], 4133 proteins were matched to five nerve-related cells: neuron, endothelium, microglia, astrocyte, and oligodendrocyte, with neuronal cells accounting for the largest proportion, followed by astrocytes (Figure 2B). Correlation analysis showed that the proteomic data were reproducible. Moreover, protein expression level in AD is negatively correlated with normal, reflecting the huge proteome difference between AD and normal tissues (Figure 2C). Two enrichment methods were used in our gene ontology (GO) analysis. According to gene count, the identified proteins were located mainly in "cytoplasm," "organelle," and "membrane" and the main molecular functions were "protein binding," "catalytic activity," and "ion binding" involved in biological processes such as "metabolism" and "transportation" (Figure 2D, Table S4). According to fold enrichment, the identified proteins were enriched mainly in "proteasome complex," "mitochondria respiratory chain," and "synaptic vesicle membrane" and the main molecular functions were "tau-protein kinase activity," "tau protein binding," and "NADH dehydrogenase activity" involved in biological processes such as "mitochondrial electron transport," "synaptic vesicle endocytosis," and "synaptic vesicle recycling" (Figure 2E, Table S4). Brain is an energy-intensive organ with high content of mitochondria. Synapse and Tau related proteins are also mainly found in the brain. From this point of view, the enrichment results based on fold enrichment could better reflect tissue function, while

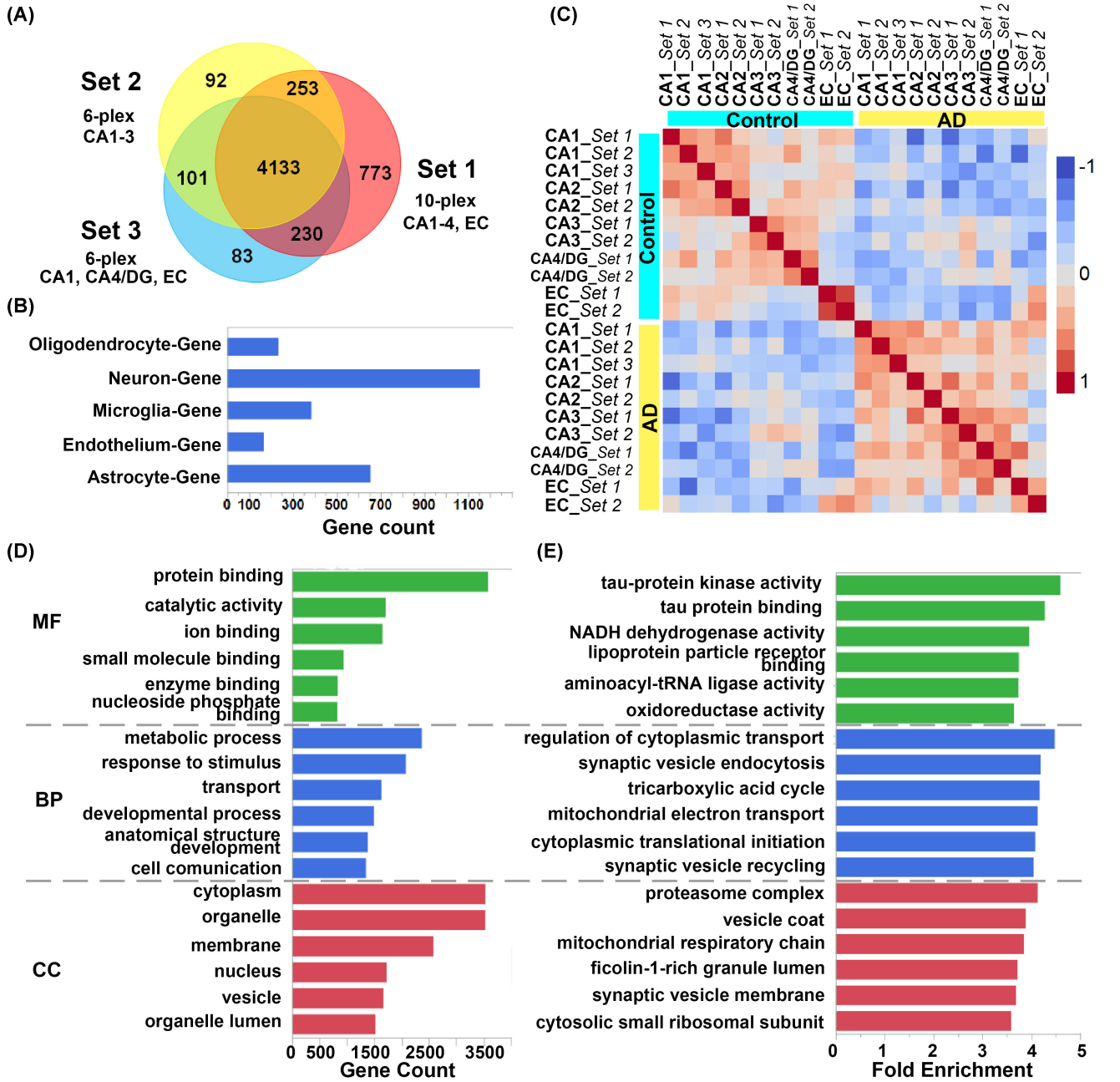

FIGURE 2 Proteomic characteristics of the total proteins identified in the hippocampus and EC. (A) Venn diagram of three sets of proteomes, including two repeat experiments. (B) Cell type analysis of 4133 proteins overlapping in three proteome sets according to the report by Zhang et al. [49]. (C) Correlation analysis of protein expression levels in ten samples using scaled abundance. (D and E) Gene ontology analysis of 4133 overlapping proteins based on the gene count (D) and fold enrichment (E)

enrichment based on gene count reflect only the basic characteristics of the proteins.

3.3 | AD-related proteins show different expression patterns in five brain regions

Disease-associated differentially expressed proteins (DEPs) were filtered with the 95% prediction interval as described in the Methods (Figure S1). The protein list of 181 DEPs is shown in Table S5. The patterns of DEPs expression in the five regions are shown in Figure 3A. Two-way cluster analysis was conducted to evaluate the distance among the five brain regions and to group proteins with similar expression profiles. The distance between the replicates in each brain region is the shortest, once again confirming that the mass spectrometry data are reproducible. The distance between the EC and the four hippocampal subfields was the farest, reflecting the differences caused by AD in different regions of

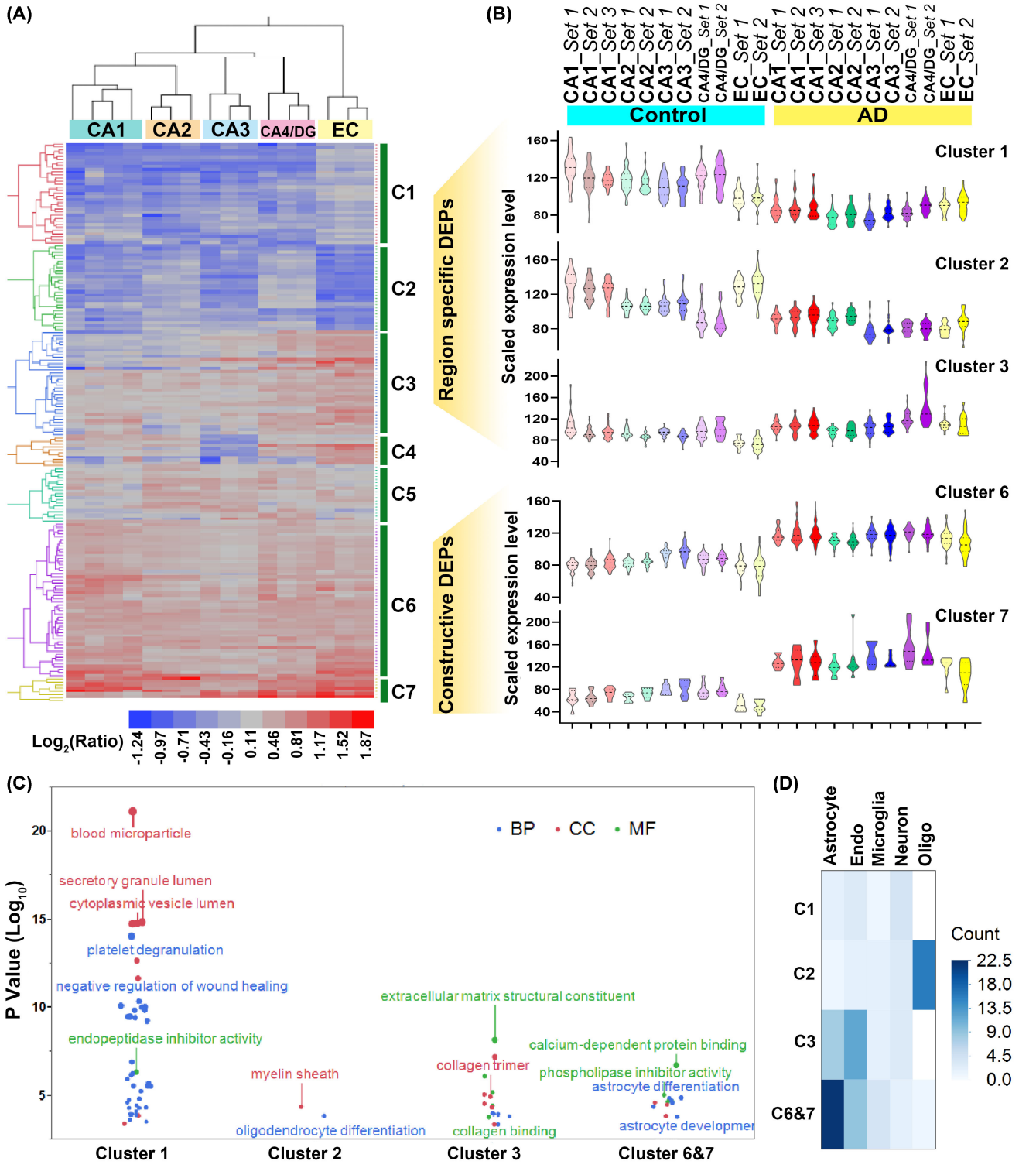

FIGURE 3 Characterization of the region-specific and region-consistent AD-associated proteins in the hippocampus and EC. (A) Heatmap of AD-associated DEPs segregated into seven clusters based on the AD/normal expression ratio. A group of average values in each brain area were added, resulting in four groups of ratios in CA1 and three groups in the other four areas. (B) Expression level of region-specific (C1–C3) and region-consistent DEPs (C6 and C7) in five brain regions of control and AD donors. (C) GO analysis of region-specific and region-consistent DEPs. (D) Cell type enrichment analysis of region-specific and region-consistent DEPs

the brain. Seven protein clusters were identified based on two-way cluster analysis. In Cluster 1 (C1), these proteins were lower expressed in CA1–CA4 of AD samples, but there is no change in the EC region. In Cluster (C2), proteins were lower expressed in CA1, CA3 and EC, with the most marked in EC region. In Cluster 3 (C3),

protein upregulation was only detected in the EC, with no changes in the other regions. In Clusters 6 and 7 (C6 and C7), proteins were upregulated in all regions. The DEPs in C1–C3 were regarded as region-specific, whereas those in C6 and C7 were regarded as region-consistent. The expression level of region-specific and region-consistent DEPs in the five regions of AD and normal donors are shown in Figure 3B. GO analysis based on fold enrichment in these region-specific and region-consistent DEPs showed that proteins in C1 were enriched in platelet deregulation and vesicle lumen, proteins in C2 were associated with myelin sheath and oligodendrocytes, proteins in C3 were related to extracellular matrix, and proteins in C6 and C7 were associated with astrocytes (Figure 3C). In accordance with the GO results, proteins in C2 were enriched in oligodendrocytes, and proteins in C6 and C7 were enriched in astrocytes (Figure 3D). For proteins in Cluster 4 and 5, they could not construct protein-protein interation network and be enriched in any GO term (Figure S2).

3.4 | The region-consistent DEPs function as a connection of different region-specific DEPs

To study the relationship between region-consistent and region-specific DEPs, we constructed a protein–protein interaction network using Cytoscape software (Figure 4). The connections of proteins in each cluster were close, while the connections of four clusters were weak, reflecting the relatively independent functions of clusters. The region-consistent DEPs (C6&7) were found to function as a bridge connecting the region-specific DEPs (C1–C3). In addition, 15 hub proteins were found in C6&7 using the cytoHubba Plug-in. Of these, eight hubs linked proteins within C6&7, and the remaining seven hub proteins connected C6&7 and clusters C1–C3.

3.5 | The S100A10-positive astrocytes increased in AD and involved in phagocytosis of apoptotic neurons

Since AD is an aging-related disease, we mapped the AD-related region-consistent DEPs (C6&7) with the aging-related proteins in the hippocampus identified in our previous study [50]. Sixteen proteins were found both aging- and AD-related (Figure 5A), with which 10 proteins were hubs (ANXA1, ANXA2, ANXA5, HSPB1, VIM, S100A10, CD44, CO1A1, COL1A2, and GFAP) indicating that these hub proteins play an important role in both AD and aging. Among these hub proteins, GFAP, VIM, and S100A10 are astrocyte markers. S100A10-positive astrocytes are thought to protect neurons by secreting neurotrophic factors [51, 52]; however, the function of S100A10-positive astrocytes in AD is unclear and other protective mechanisms may also exist.

Our IHC and IF analyses revealed that S100A10 is expressed in some small astrocyte-like cells in the normal donors. The enlarged cell bodies and greater degree of branching indicated that these S100A10-positive astrocytes are activated in AD patients (Figure 5B,C). In addition, the number of S100A10-positive astrocytes was significantly increased in all five regions of pre-AD and AD donors (Figure 5D). Similarly, the number of S100A10-positive astrocytes was highest in the donors with the most severe pathology reflected by an ABC score of "H" (Figure 5E).

Because S100A10-positive astrocytes are regarded as neuroprotective glial cells, we next investigated the relationship between S100A10-positive astrocytes and neurons using dual immunofluorescence staining. In normal donors, NeuN, a neuron marker, was expressed at high levels in both the cytoplasm and the nucleus of neurons. In pre-AD and AD samples, the NeuN signal was weak, concentrated in the cytoplasm, with negligible staining in the nucleus (Figure 6A–C, Figure S3). This result is consistent with previously reports that NeuN is expressed at low levels in AD [53], and localized mainly in the cytoplasm in HIV-infected individuals with cognitive impairment [54]. In addition, we also detected a large number of NeuN-positive debris in pre-AD and AD donors, but not in normal donors. This debris was surrounded by S100A10-positive astrocytes and some of them were enclosed by astrocytes (Figure 6A–C, Figures S3 and S4). We named these astrocytes as phagocytic S100A10-positive astrocytes. The number and percentage of these phagocytic S100A10-positive astrocytes increased significantly in pre-AD and AD donors (Figure 6D,E). It was further found that the NeuN-positive debris co-localized with the apoptosis marker cleaved caspase-3 (Figure 6F–H), indicating that the debris was derived from apoptotic neurons. Similar results were also observed using antibodies for the detection of APP and Aβ, which are mainly expressed in neurons (Figures S5 and S6).

3.6 | Oligodendrocyte and myelin sheath density are reduced in pre-AD in a region-specific manner

For the region-specific DEPs, all C2 proteins were enriched in oligodendrocyte differentiation and myelin sheath formation. As shown in Figure 7A, these proteins were lowest expressed in the EC, followed by CA1 and CA3. For further IHC analysis, we selected CNP, which is expressed both in pre-oligodendrocytes and mature oligodendrocytes (myelin sheath), and MBP, which is mainly expressed in myelin sheath. The IHC results showed that the expression of CNP and MBP were both reduced in the pre-AD and AD group in the EC region (Figure 7B), with statistically significant in AD pathology and pre-AD group (Figure 7C,D). However, there

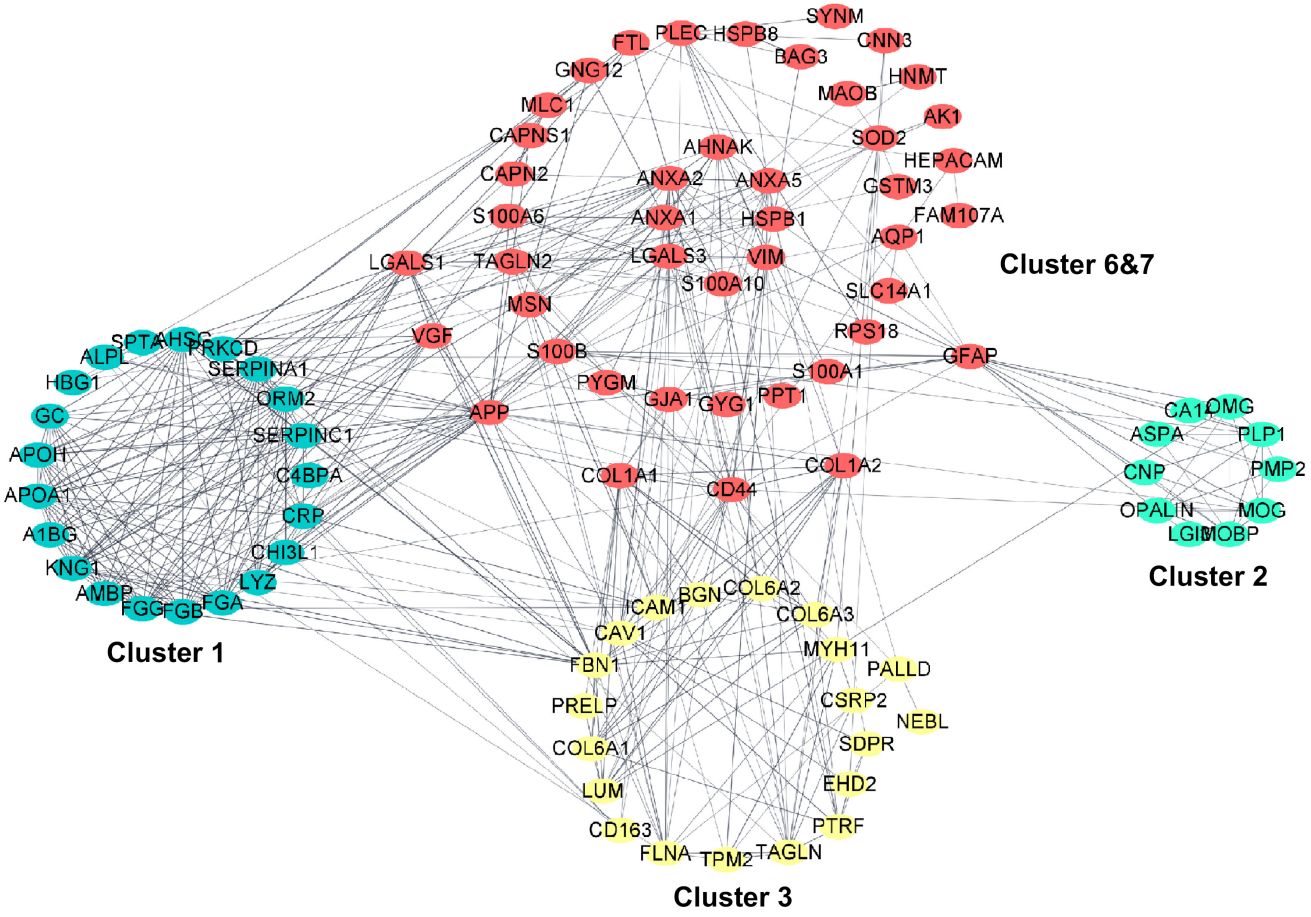

FIGURE 4 Protein-protein interaction network of region-specific and region-consistent DEPs

were no significant differences in the expression of MBP and CNP among normal, AD pathology, pre-AD, and AD groups in other regions (Table S6).

4 | DISCUSSION

Few studies of AD or other neuropsychiatric disorders have focused on the molecular differences between hippocampal subfields, except that von Ziegler et al. reported marked differences in the protein profiles of CA1 and CA3 in normal mice, no matter under basal conditions (untreated or stimulated) or memory formation conditions (object recognition and object location recognition) [55]. Hence, we hypothesized that the characteristic dynamic protein changes in subfields of the hippocampus may reflect the regional differences caused by AD. In this study, we compared the protein profiles of the hippocampal subfields in postmortem brain tissues from AD and normal donors. We found differences in the expression levels among the hippocampal subfields of normal donors (Figure 3B, Figure S7), indicating that in studies of larger or heterogeneous brain regions (such as the hippocampus), the same subregions should be compared to minimize the bias due to tissue selection. Furthermore, we found regional specificity in the dynamic changes in protein expression associated with AD (Figure 2B). For example, oligodendrocytes and myelin-associated proteins were expressed significantly lower in the EC regions of AD patients, while no significant change was observed in the other regions (Figure 7), indicating the existence of regional differences in the responses of the brain in AD.

The lower expression of oligodendrocyte- or myelin-associated proteins suggests myelin loss, which is associated with Aβ deposition, Tau pathology, and cognitive decline [56–58]. Bartzokis et al. suggested that myelin breakdown and degeneration of oligodendrocytes resulted in the release of substantial amounts of stored iron that, in the absence of effective clearance, accumulated in the brain leading to increased Aβ production and deposition [56, 59]. Besides, the Aβ oligomers and fibers also stimulate demyelination and oligodendrocyte apoptosis [60]. This vicious cycle further exacerbates Aβ deposition and demyelination, leading to cognitive decline. It can be speculated that a more severe pathological alteration in the CA1 and EC [18] is caused by an increased susceptibility of the oligodendrocytes to Aβ oligomers in these

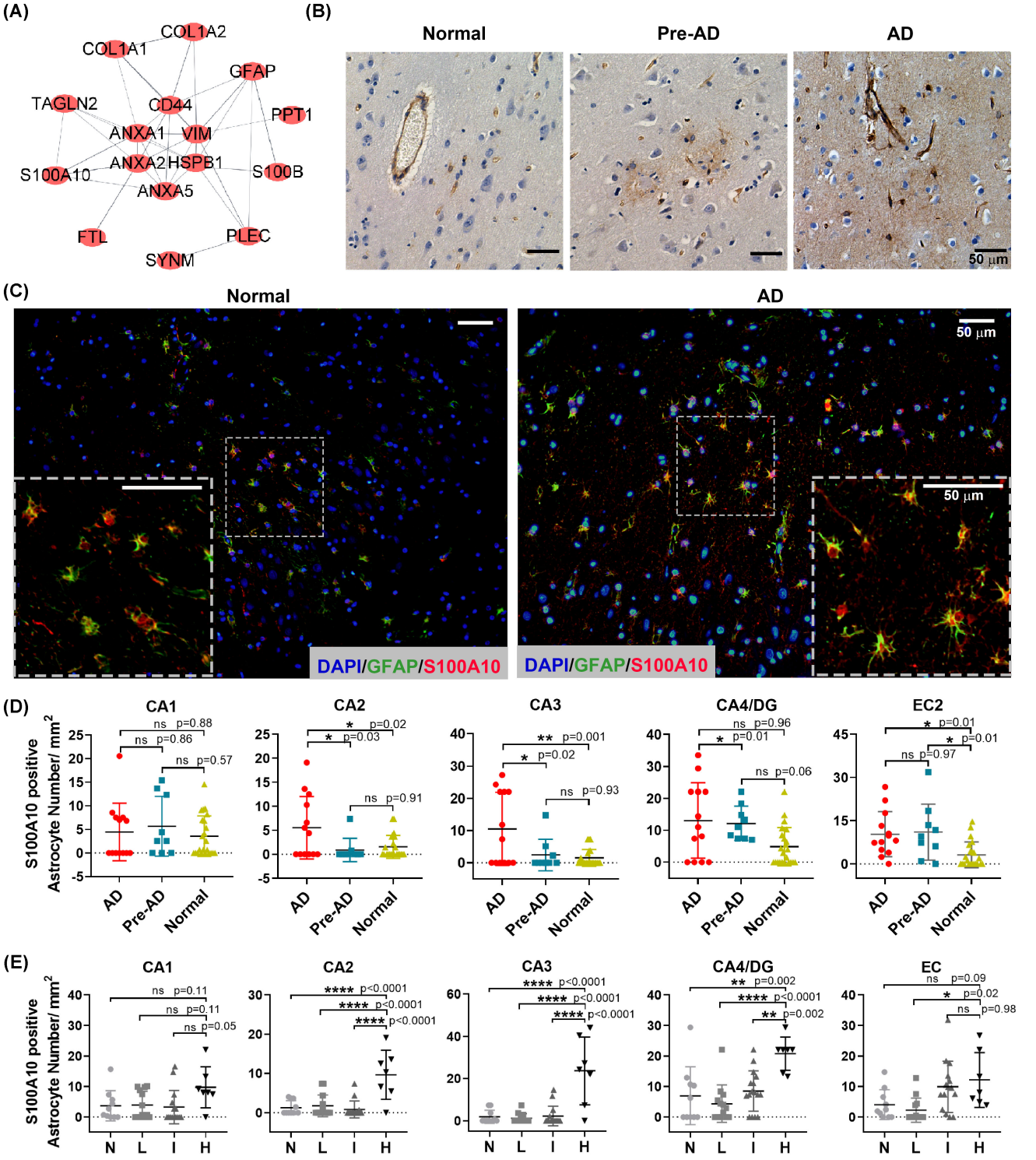

FIGURE 5 The numbers of S100A10-positive astrocytes increase in all hippocampal subfields and EC region in AD. (A) The protein-protein interaction network of DEPs shared by AD and aging. (B) Representative images of IHC staining of S100A10 in the EC area in normal, Pre-AD and AD specimens. Scale bar: 50 μm. (C) Representative immunofluorescence images of dual staining of S100A10 and GFAP in the EC area of normal, Pre-AD and AD specimens. Red, S100A10-positive astrocytes; green, GFAP-positive astrocytes. Insets are higher magnification images, Scale bar: 50 μm. (D) Scatter plot of the normalized S100A10 positive astrocytes number in the normal, Pre-AD and AD group in the hippocampal subregion and EC region. (E) Scatter plot of the normalized S100A10-positive astrocytes number in ABC score groups (N, L, I or H) in hippocampal subfields and EC region. The cell counting in D and E is based on IHC staining of S100A10, using 22 case normal, 9 case pre-AD and 13 case AD. The number of S100A10-positive astrocytes shown in the figure is normalized with area (per mm^2). One-way ANOVA was used to compare the number of cells in the three groups, and the *p*-value is shown in the figure. $*p < 0.05$; $**p < 0.01$; $***p < 0.001$; $****p < 0.0001$

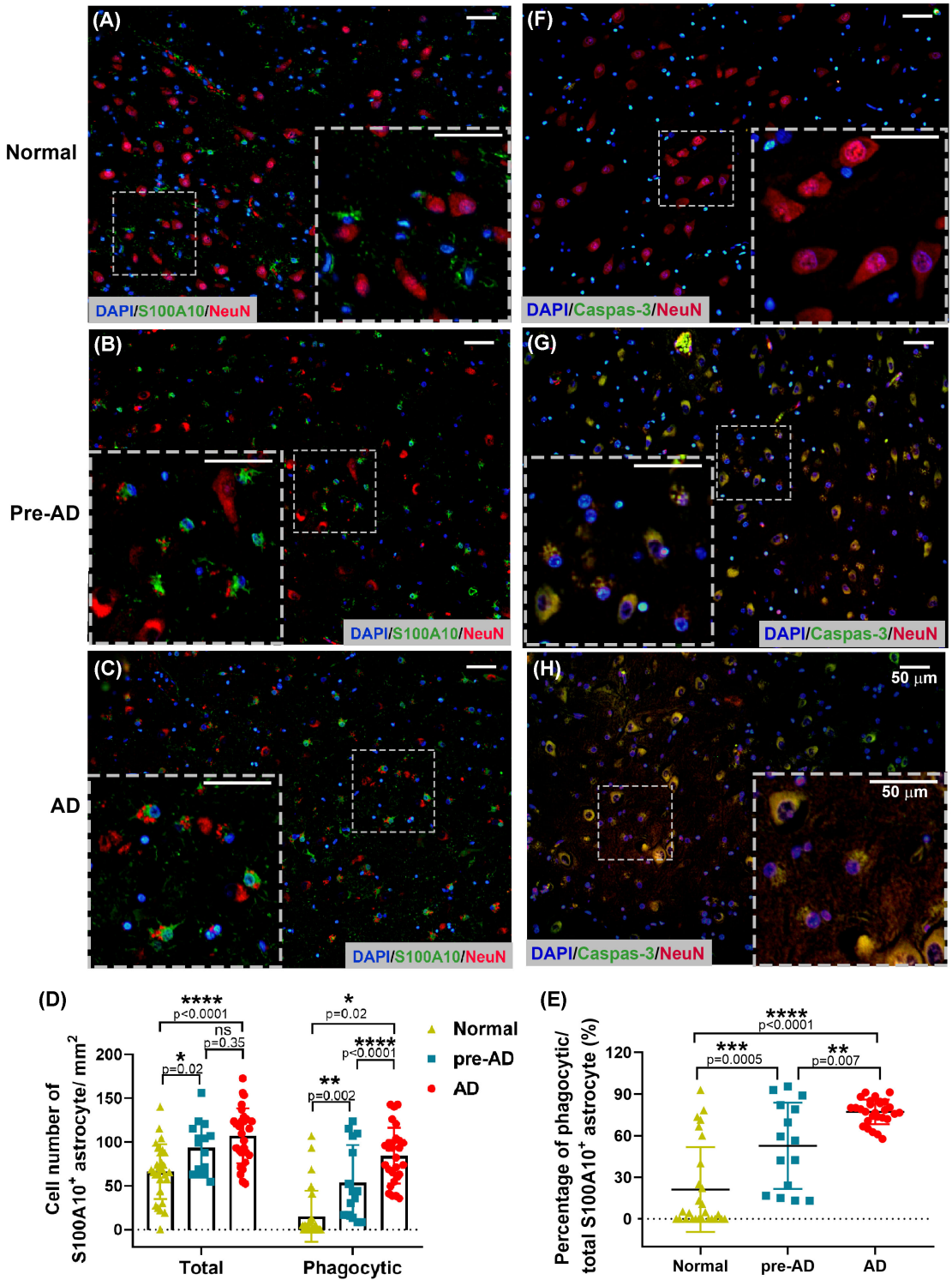

FIGURE 6 S100A10-positive astrocytes contain apoptotic neuron debris. (A–C) Dual immunofluorescence staining of S100A10 and NeuN in CA4/DG region of normal, Pre-AD and AD specimens. The results of other subfields are shown in the Figure S3. Red, NeuN-positive neurons; green, S100A10-positive astrocytes. Scale bar: 50 μm. (D) Normalized cell number of total and neuron phagocytic S100A10-positive astrocytes in normal ($n = 3$), Pre-AD ($n = 2$) and AD ($n = 3$) specimens. The number of cells shown in the figure is normalized with area (per mm^2). (E) The scatter plot of percentage of phagocytic S100A10 positive astrocytes in normal, Pre-AD and AD specimens. (F–H), Dual immunofluorescence staining of cleaved caspase-3 and NeuN in CA4/DG region of normal, Pre-AD and AD specimens. Red, NeuN-positive neurons; green, Caspase-3 positive signaling. Scale bar: 50 μm. One-way ANOVA is used to compare the cell number or percentage among normal, pre-AD and AD group, and the p-value is shown in the figure. *$p < 0.05$; **$p < 0.01$; ***$p < 0.001$; ****$p < 0.0001$

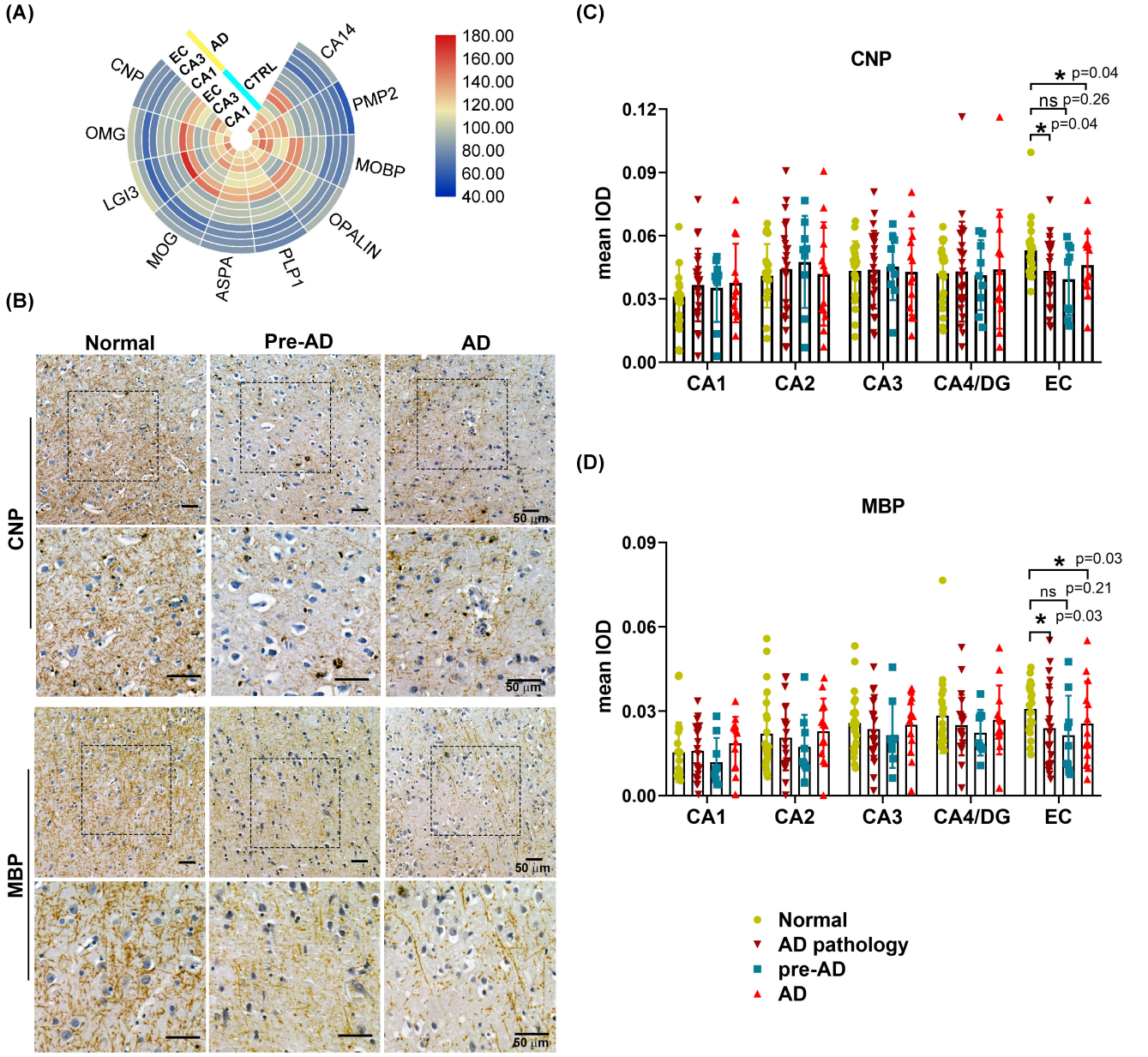

FIGURE 7 Region-specific low expression of oligodendrocyte and myelin-associated proteins. (A) Heatmap of myelin-associated proteins in CA1, CA3 and the EC regions. The Color intensity represents protein abundance. (B) Representative image of IHC staining of MBP and CNP in the EC region of normal, Pre-AD and AD specimens. Scale bar: 50 μm. (C and D) Expression intensity of MBP and CNP proteins in each area in normal, Pre-AD and AD specimens. The intensity was calculated based on grayscale values using Image-Pro Plus 6.0 software. Mean IOD: mean integrated optical density. One-way ANOVA is used to compare the mean IOD among normal, pre-AD and AD group in each brain region. There is no significant difference among normal, pre-AD and AD group in CA1–CA4/DG regions. The *p*-value of CA1–CA4/DG region is shown in Table S6. $*p < 0.05$

areas. Recent studies in a mouse model of AD has confirmed myelin loss in the hippocampus and illuminated that enhancement of myelin renewal alleviated cognitive impairment [61], which directly proved the important role of hippocampal myelin in cognition. Our results suggest that the myelin loss in CA1, CA3, and the EC plays a pivotal role in the cognitive decline.

Our analysis of hippocampal subfields also revealed a uniform increase in the number of S100A10-positive astrocytes in all five subregions, suggesting that proliferation of this population in the hippocampus is closely related to AD. S100A10-positive astrocytes, which were first identified in mice, are considered to have neuroprotective efficacy and to be activated under hypoxic conditions to promote neuron growth [51, 52]. Previous studies have also showed that S100A10-positive astrocytes are proliferated and activated in AD patients [62], but their role in AD pathogenesis is unclear. As astrocytes are a heterogeneous population, the characteristics of S100A10-positive astrocytes remain

to be clarified. In this study, we found that S100A10-positive astrocytes are small, and these cells do not surround Aβ, with no obvious aggregation (Figure S8). In contrast, as reported by Pike et al., GFAP-positive reactive astrocytes are larger in shape and entangled around Aβ plaques [63]. Further relationship between S100A10-positive astrocytes and neurons was also explored, revealing that S100A10-positive astrocytes were surrounded by the NeuN-positive debris of neurons. These debris are also co-stained with an apoptotic marker cleaved caspase 3. The confocal results displayed that part of the NeuN-positive debris was enclosed by S100A10-positive astrocytes (Figure S4), indicating that these astrocytes may undergo phagocytosis of the neuron debris resulting from cell apoptosis. Gomez–Arboledas et al. found that GFAP-positive reactive astrocytes contained APP-positive fragments, which was thought to be the result of phagocytic clearance of presynaptic dystrophies by reactive astrocytes [64]. We also found that S100A10-positive astrocytes phagocytosed APP-positive fragments (Figure S5). These results support the hypothesis that S100A10-positive astrocytes may play a neuroprotective role by phagocytosing apoptotic neurons, thereby reducing the damage to surrounding tissues and inhibiting the immune response and pathological progress. Further studies in mouse models are required to verify this hypothesis and fully elucidate the specific mechanisms.

Our results highlight the role of glial cells, oligodendrocytes and astrocytes, in AD. However, microglia-related process were not enriched by DEPs, which may partly attribute to that the changes in hippocampal microglia caused by AD are weaker than those in astrocytes and oligodendrocytes, thus the alterations are masked in the proteomic analyses.

In addition to glial cell-related proteins, we also found that extracellular matrix proteins were higher expressed in AD, especially in the EC region (Cluster 3, Figure 4). These extracellular matrix proteins were mainly enriched in endothelial cells, which was probably a consequence of vascular disease which could result in AD [65, 66]. Among these proteins, type I and type VI collagen have been reported to play a neuroprotective role by hindering the binding of Aβ to neurons [67] and inhibiting neuronal apoptosis [68]. Caveolin-1, which is upregulated in AD [69], may also play a neuroprotective role, and as displayed by previous study, its loss exacerbates neurodegeneration [70]. TPM2, ICAM1, and biglycans are entangled in the neurofibrillary tangles and the senile plaques of AD patients [71–73]. FLNA is involved in the process by which Aβ activates Tau phosphorylation and immune response in neurons [70]. CD163 identifies a unique population of ramified microglia [74], and its expression is elevated in AD [75]. Genome-wide association studies have indicated that NEBL, EHD2, LUM, and FBN1 are related to AD. The remaining proteins in Cluster 3 identified in this study have not been reported to be involved in AD or other neurodegenerative diseases.

Despite the strengths of the study, the limitations of this study should be noted. As Chinese brain bank has just been established for 9 years since 2012, there are only 400 cases of human brain tissue in the bank, including 40 cases with AD pathology. The research of Chinese race-specific brain tissue is almost at a blank stage in the world, and the research of molecular pathology based on the Chinese human brain has just started. Hence, one limitation of this study is the relatively small sample size used in proteomic analysis. To mitigate this limitation, immunohistochemical analysis containing 44 cases and dual immunofluorescence of 17 cases were performed in our study.

Proteomics provides the possibility to study large number of molecular changes in scarce samples. There are many strategies for quantitative proteomics research, and each strategy has its advantages and disadvantages [76, 77]. Label free can perform high-throughput individual proteomics analysis, but the number of identified proteins is limited; while *in vitro* labels, such as TMT or iTRAQ, provide high quantitative accuracy, and the number of identified proteins is 3–5 times higher than that of label free; however, the number of samples tested per experiment is limited. Thus, mixed sample strategy was usually used. In our research, the use of TMT-based quantitative proteomics could provide more abundant and accurate protein quantitative information.

A common problem with human tissue samples is that there are large individual differences, which may be caused by individual characteristics and the nonuniformity in the process of brain collecting. Due to the relatively small sample size at this stage and the relatively large variation between samples, some inevitable errors may occur in the current results, which may lead to bias in the interpretation.

Based on the current limitation, this study uses TMT-based proteomics technology to maximize the number of identified proteins and obtain more quantitative information. Due to the relatively small sample size, the limitations of proteomics technology and the relatively large individual differences in humans, the interpretation of the results may be biased. In addition, this descriptive research is based mainly on postmortem human brain tissue, which limits a sufficiently rigorous approach to the causation. Further studies in animal models are required to explore the specific role of S100A10-positive astrocytes in AD, including the potential of these cells to improve cognition, and the mechanism by which they phagocytose apoptotic neurons.

ACKNOWLEDGMENTS

Tissues were provided by National Human Brain Bank for Development and Function, Chinese Academy of Medical Sciences and Peking Union Medical College, Beijing, China. This study was supported by the Institute

of Basic Medical Sciences, Chinese Academy of Medical Sciencesss, Neuroscience Center, and the China Human Brain Banking Consortium. Thanks to Dr. Wenying Qiu for her guidance on pathological knowledge.

CONFLICT OF INTEREST

The authors declare that they have no conflict of interests.

AUTHOR CONTRIBUTIONS

Yanpan Gao performed bioinformatic analysis, experiment design, figure arrangement, and draft writing. Jiaqi Liu and Yifan Liu performed IHC and IF experiment. Jiayu Wang performed tissue collection and TMT-based quantitative proteomics experiment. Ling-Hui Zeng, Wei Ge, and Chao Ma designed this project and polished the manuscript.

ETHICS APPROVAL AND CONSENT TO PARTICIPATE

This study was approved by the ethics committee of The Institute of Basic Medical Sciences of the Chinese Academy of Medical Sciences (Approval Number: 009-2014).

CONSENT FOR PUBLICATION

The informed consent of the donor or family member has been obtained.

DATA AVAILABILITY STATEMENT

The mass spectrometry proteomics data have been deposited to the ProteomeXchange Consortium (http://proteomecentral.proteomexchange.org) with the dataset identifier PXD027380. All the other data generated or analyzed during this study are included in this published article and its Supporting Information files.

ORCID

Wei Ge https://orcid.org/0000-0002-9907-512X

REFERENCES

1. Scheltens P, De Strooper B, Kivipelto M, Holstege H, Chételat G, Teunissen CE, et al. Alzheimer's disease. Lancet. 2021;397:1577–90.
2. Rajan KB, Weuve J, Barnes LL, Wilson RS, Evans DA. Prevalence and incidence of clinically diagnosed Alzheimer's disease dementia from 1994 to 2012 in a population study. Alzheimers Dement. 2019;15:1–7.
3. Alzheimer's Disease International, Patterson C. World Alzheimer report. 2018.
4. Alzheimer's Association. Alzheimer's disease facts and figures. 2021.
5. Serrano-Pozo A, Frosch MP, Masliah E, Hyman BT. Neuropathological alterations in Alzheimer disease. Cold Spring Harb Perspect Med. 2011;1:a006189.
6. Vaz M, Silvestre S. Alzheimer's disease: recent treatment strategies. Eur J Pharmacol. 2020;887:173554.
7. Mullard A. Failure of first anti-tau antibody in Alzheimer disease highlights risks of history repeating. Nat Rev Drug Discovery. 2021;20:3–5.
8. Alexander GC, Emerson S, Kesselheim AS. Evaluation of aducanumab for Alzheimer disease: scientific evidence and regulatory review involving efficacy, safety, and futility. JAMA. 2021;325:1717–8.
9. Yankner BA. Mechanisms of neuronal degeneration in Alzheimer's disease. Neuron. 1996;16:921–32.
10. Vickers JC, Mitew S, Woodhouse A, Fernandez-Martos CM, Kirkcaldie MT, Canty AJ, et al. Defining the earliest pathological changes of Alzheimer's disease. Curr Alzheimer Res. 2016;13:281–7.
11. Henstridge CM, Hyman BT, Spires-Jones TL. Beyond the neuron–cellular interactions early in Alzheimer disease pathogenesis. Nat Rev Neurosci. 2019;20:94–108.
12. Sarlus H, Heneka MT. Microglia in Alzheimer's disease. J Clin Invest. 2017;127:3240–9.
13. Arranz AM, De Strooper B. The role of astroglia in Alzheimer's disease: pathophysiology and clinical implications. Lancet Neurol. 2019;18:406–14.
14. Nasrabady SE, Rizvi B, Goldman JE, Brickman AM. White matter changes in Alzheimer's disease: a focus on myelin and oligodendrocytes. Acta Neuropathol Commun. 2018;6:22.
15. Grubman A, Chew G, Ouyang JF, Sun G, Choo XY, McLean C, et al. A single-cell atlas of entorhinal cortex from individuals with Alzheimer's disease reveals cell-type-specific gene expression regulation. Nat Neurosci. 2019;22:2087–97.
16. Reilly JF, Games D, Rydel RE, Freedman S, Schenk D, Young WG, et al. Amyloid deposition in the hippocampus and entorhinal cortex: Quantitative analysis of a transgenic mouse model. Proc Natl Acad Sci U S A. 2003;100:4837–42.
17. West MJ, Coleman PD, Flood DG, Troncoso JC. Differences in the pattern of hippocampal neuronal loss in normal ageing and Alzheimer's disease. Lancet. 1994;344:769–72.
18. Braak H, Braak E. Neuropathological stageing of Alzheimer-related changes. Acta Neuropathol. 1991;82:239–59.
19. De Flores R, La Joie R, Landeau B, Perrotin A, Mézenge F, De La Sayette V, et al. Effects of age and Alzheimer's disease on hippocampal subfields. Hum Brain Mapp. 2015;36:463–74.
20. Chételat G, Fouquet M, Kalpouzos G, Denghien I, De La Sayette V, Viader F, et al. Three-dimensional surface mapping of hippocampal atrophy progression from MCI to AD and over normal aging as assessed using voxel-based morphometry. Neuropsychologia. 2008;46:1721–31.
21. Diehl GW, Hon OJ, Leutgeb S, Leutgeb JK. Grid and nongrid cells in medial entorhinal cortex represent spatial location and environmental features with complementary coding schemes. Neuron. 2017;94:83–92.e86.
22. Garcia AD, Buffalo EA. Anatomy and function of the primate entorhinal cortex. Annu Rev Vis Sci. 2020;6:411–32.
23. Rozov A, Rannap M, Lorenz F, Nasretdinov A, Draguhn A, Egorov AV. Processing of hippocampal network activity in the receiver network of the medial entorhinal cortex layer V. J Neurosci. 2020;40:8413–25.
24. Long JM, Holtzman DM. Alzheimer disease: an update on pathobiology and treatment strategies. Cell. 2019;179:312–39.
25. Márquez F, Yassa MA. Neuroimaging biomarkers for Alzheimer's disease. Mol Neurodegener. 2019;14:21.
26. Rayment D, Biju M, Zheng R, Kuruvilla T. Neuroimaging in dementia: an update for the general clinician. Prog Neurol Psychiatry. 2016;20:16–20.
27. Ying Y, Wang J-Z. Illuminating neural circuits in Alzheimer's disease. Neurosci Bull. 2021;37:1203–17.
28. Rehiman SH, Lim SM, Neoh CF, Majeed ABA, Chin AV, Tan MP, et al. Proteomics as a reliable approach for discovery of blood-based Alzheimer's disease biomarkers: a systematic review and meta-analysis. Ageing Res Rev. 2020;60:101066.
29. Elahi FM, Casaletto KB, La Joie R, Walters SM, Harvey D, Wolf A, et al. Plasma biomarkers of astrocytic and neuronal dysfunction in early- and late-onset Alzheimer's disease. Alzheimers Dement. 2020;16:681–95.

30. Sathe G, Na CH, Renuse S, Madugundu AK, Albert M, Moghekar A, et al. Quantitative proteomic profiling of cerebrospinal fluid to identify candidate biomarkers for Alzheimer's disease. Proteomics Clin Appl. 2019;13:1800105.
31. Muraoka S, Jedrychowski MP, Yanamandra K, Ikezu S, Gygi SP, Ikezu T. Proteomic profiling of extracellular vesicles derived from cerebrospinal fluid of Alzheimer's disease patients: a pilot study. Cells. 2020;9:1959.
32. Muraoka S, Deleo AM, Sethi MK, Yukawa-Takamatsu K, Yang Z, Ko J, et al. Proteomic and biological profiling of extracellular vesicles from Alzheimer's disease human brain tissues. Alzheimers Dement. 2020;16:896–907.
33. Jia Y, Wang X, Chen Y, Qiu W, Ge W, Ma C. Proteomic and transcriptomic analyses reveal pathological changes in the entorhinal cortex region that correlate well with dysregulation of ion transport in patients with alzheimer's disease. Mol Neurobiol. 2021;58:4007–27.
34. Mendonça CF, Kuras M, Nogueira FCS, Plá I, Hortobágyi T, Csiba L, et al. Proteomic signatures of brain regions affected by tau pathology in early and late stages of Alzheimer's disease. Neurobiol Dis. 2019;130:104509.
35. Liu X, Guo Z, Liu W, Sun W, Ma C. Differential proteome analysis of hippocampus and temporal cortex using label-free based 2D-LC-MS/MS. J Proteomics. 2017;165:26–34.
36. Sultana R, Boyd-Kimball D, Cai J, Pierce WM, Klein JB, Merchant M, et al. Proteomics analysis of the Alzheimer's disease hippocampal proteome. J Alzheimers Dis. 2007;11:153–64.
37. Di Domenico F, Sultana R, Barone E, Perluigi M, Cini C, Mancuso C, et al. Quantitative proteomics analysis of phosphorylated proteins in the hippocampus of Alzheimer's disease subjects. J Proteomics. 2011;74:1091–103.
38. Sultana R, Boyd-Kimball D, Poon HF, Cai J, Pierce WM, Klein JB, et al. Redox proteomics identification of oxidized proteins in Alzheimer's disease hippocampus and cerebellum: an approach to understand pathological and biochemical alterations in AD. Neurobiol Aging. 2006;27:1564–76.
39. Bai B, Wang X, Li Y, Chen PC, Yu K, Dey KK, et al. Deep multilayer brain proteomics identifies molecular networks in Alzheimer's disease progression. Neuron. 2020;105:975–991.e977.
40. Verkhratsky A, Zorec R. Large-scale proteomics highlights glial role in neurodegeneration. Cell Metab. 2020;32:11–2.
41. Xu L, Sun H, Zhang Y, Guo Z, Xiao X, Zhou X, et al. Proteomic analysis of human frontal and temporal cortex using iTRAQ-based 2D LC-MS/MS. Chin Neurosurg J. 2021;7:27.
42. Dubois B, Hampel H, Feldman HH, Scheltens P, Aisen P, Andrieu S, et al. Preclinical Alzheimer's disease: definition, natural history, and diagnostic criteria. Alzheimers Dement. 2016;12:292–323.
43. Samarasekera N, Salman RA-S, Huitinga I, Klioueva N, McLean CA, Kretzschmar H, et al. Brain banking for neurological disorders. Lancet Neurol. 2013;12:1096–105.
44. Farias ST, Mungas D, Reed BR, Cahn-Weiner D, Jagust W, Baynes K, et al. The measurement of everyday cognition (ECog): scale development and psychometric properties. Neuropsychology. 2008;22:531–44.
45. Hyman BT, Phelps CH, Beach TG, Bigio EH, Cairns NJ, Carrillo MC, et al. National Institute on Aging-Alzheimer's Association guidelines for the neuropathologic assessment of Alzheimer's disease. Alzheimers Dement. 2012;8:1–13.
46. Ghose S, Winter MK, McCarson KE, Tamminga CA, Enna SJ. The $GABA_B$ receptor as a target for antidepressant drug action. Br J Pharmacol. 2011;162:1–17.
47. Perez JM, Berto S, Gleason K, Ghose S, Tan C, Kim TK, et al. Hippocampal subfield transcriptome analysis in schizophrenia psychosis. Mol Psychiatry. 2021;26:2577–89.
48. Ma J, Chen T, Wu S, Yang C, Bai M, Shu K, et al. iProX: an integrated proteome resource. Nucleic Acids Res. 2019;47:D1211–7.
49. Zhang Y, Sloan SA, Clarke LE, Caneda C, Plaza CA, Blumenthal PD, et al. Purification and characterization of progenitor and mature human astrocytes reveals transcriptional and functional differences with mouse. Neuron. 2016;89:37–53.
50. Xu B, Gao Y, Zhan S, Xiong F, Qiu W, Qian X, et al. Quantitative protein profiling of hippocampus during human aging. Neurobiol Aging. 2016;39:46–56.
51. Zamanian JL, Xu L, Foo LC, Nouri N, Zhou L, Giffard RG, et al. Genomic analysis of reactive astrogliosis. J Neurosci. 2012;32:6391–410.
52. Liddelow SA, Guttenplan KA, Clarke LE, Bennett FC, Bohlen CJ, Schirmer L, et al. Neurotoxic reactive astrocytes are induced by activated microglia. Nature. 2017;541:481–7.
53. Zhou L, Wei C, Huang W, Bennett DA, Dickson DW, Wang R, et al. Distinct subcellular patterns of neprilysin protein and activity in the brains of Alzheimer's disease patients, transgenic mice and cultured human neuronal cells. Am J Transl Res. 2013;5:608–21.
54. Gusel'nikova VV, Korzhevskiy DE. NeuN as a neuronal nuclear antigen and neuron differentiation marker. Acta Naturae. 2015;7:42–7.
55. von Ziegler LM, Selevsek N, Tweedie-Cullen RY, Kremer E, Mansuy IM. Subregion-specific proteomic signature in the hippocampus for recognition processes in adult mice. Cell Rep. 2018;22:3362–74.
56. Bartzokis G, Lu PH, Mintz J. Human brain myelination and amyloid beta deposition in Alzheimer's disease. Alzheimers Dement. 2007;3:122–5.
57. Desai MK, Mastrangelo MA, Ryan DA, Sudol KL, Narrow WC, Bowers WJ. Early oligodendrocyte/myelin pathology in Alzheimer's disease mice constitutes a novel therapeutic target. Am J Pathol. 2010;177:1422–35.
58. Papuć E, Rejdak K. The role of myelin damage in Alzheimer's disease pathology. Arch Med Sci. 2018;16:345–51.
59. Uranga RM, Salvador GA. Unraveling the burden of iron in neurodegeneration: intersections with amyloid beta peptide pathology. Oxid Med Cell Longev. 2018;2018:2850341.
60. Lee J-T, Xu J, Lee J-M, Ku G, Han X, Yang D-I, et al. Amyloid-beta peptide induces oligodendrocyte death by activating the neutral sphingomyelinase-ceramide pathway. J Cell Biol. 2004;164:123–31.
61. Chen J-F, Liu K, Hu B, Li R-R, Xin W, Chen H, et al. Enhancing myelin renewal reverses cognitive dysfunction in a murine model of Alzheimer's disease. Neuron. 2021;109:2292–307.e5.
62. King A, Szekely B, Calapkulu E, Ali H, Rios F, Jones S, et al. The increased densities, but different distributions, of both C3 and S100A10 immunopositive astrocyte-like cells in Alzheimer's disease brains suggest possible roles for both A1 and A2 astrocytes in the disease pathogenesis. Brain Sci. 2020;10:503.
63. Pike CJ, Cummings BJ, Monzavi R, Cotman CW. Beta-amyloid-induced changes in cultured astrocytes parallel reactive astrocytosis associated with senile plaques in Alzheimer's disease. Neuroscience. 1994;63:517–31.
64. Gomez-Arboledas A, Davila JC, Sanchez-Mejias E, Navarro V, Nuñez-Diaz C, Sanchez-Varo R, et al. Phagocytic clearance of presynaptic dystrophies by reactive astrocytes in Alzheimer's disease. Glia. 2018;66:637–53.
65. Amtul Z, Frías C, Randhawa J, Hill DJ, Arany EJ. Spatial dynamics of vascular and biochemical injury in rat hippocampus following striatal injury and Aβ toxicity. Mol Neurobiol. 2019;56:2714–27.
66. Amtul Z, Nikolova S, Gao L, Keeley RJ, Bechberger JF, Fisher AL, et al. Comorbid Aβ toxicity and stroke: hippocampal atrophy, pathology, and cognitive deficit. Neurobiol Aging. 2014;35:1605–14.
67. Cheng JS, Dubal DB, Kim DH, Legleiter J, Cheng IH, Yu G-Q, et al. Collagen VI protects neurons against Abeta toxicity. Nat Neurosci. 2009;12:119–21.
68. Cescon M, Chen P, Castagnaro S, Gregorio I, Bonaldo P. Lack of collagen VI promotes neurodegeneration by impairing

autophagy and inducing apoptosis during aging. Aging (Albany NY). 2016;8:1083–101.
69. Gaudreault SB, Dea D, Poirier J. Increased caveolin-1 expression in Alzheimer's disease brain. Neurobiol Aging. 2004;25:753–9.
70. Head BP, Peart JN, Panneerselvam M, Yokoyama T, Pearn ML, Niesman IR, et al. Loss of caveolin-1 accelerates neurodegeneration and aging. PLoS One. 2010;5:e15697.
71. Galloway PG, Mulvihill P, Siedlak S, Mijares M, Kawai M, Padget H, et al. Immunochemical demonstration of tropomyosin in the neurofibrillary pathology of Alzheimer's disease. Am J Pathol. 1990;137:291–300.
72. Verbeek MM, Otte-Höller I, Westphal JR, Wesseling P, Ruiter DJ, de Waal RM. Accumulation of intercellular adhesion molecule-1 in senile plaques in brain tissue of patients with Alzheimer's disease. Am J Pathol. 1994;144:104–16.
73. Snow AD, Kinsella MG, Parks E, Sekiguchi RT, Miller JD, Kimata K, et al. Differential binding of vascular cell-derived proteoglycans (perlecan, biglycan, decorin, and versican) to the beta-amyloid protein of Alzheimer's disease. Arch Biochem Biophys. 1995;320:84–95.
74. Roberts ES, Masliah E, Fox HS. CD163 identifies a unique population of ramified microglia in HIV encephalitis (HIVE). J Neuropathol Exp Neurol. 2004;63:1255–64.
75. Pey P, Pearce RK, Kalaitzakis ME, Griffin WS, Gentleman SM. Phenotypic profile of alternative activation marker CD163 is different in Alzheimer's and Parkinson's disease. Acta Neuropathol Commun. 2014;2:21.
76. Megger DA, Pott LL, Ahrens M, Padden J, Bracht T, Kuhlmann K, et al. Comparison of label-free and label-based strategies for proteome analysis of hepatoma cell lines. Biochim Biophys Acta. 2014;1844:967–76.
77. Bantscheff M, Schirle M, Sweetman G, Rick J, Kuster B. Quantitative mass spectrometry in proteomics: a critical review. Anal Bioanal Chem. 2007;389:1017–31.

SUPPORTING INFORMATION

Additional supporting information may be found in the online version of the article at the publisher's website.

Fig S1-S8

FIGURE S1 The 95% prediction interval of total protein ratios in the 6-plex (A) and 10-plex (B) labeled proteome data

FIGURE S2 The protein-protein network in Cluster 4 (A) and Cluster 5 (B)

FIGURE S3 Representative images of dual immunofluorescence staining of S100A10 and NeuN in the CA1, CA2, CA3 and EC regions of cognitively normal, Pre-AD and AD donors. Red, NeuN-positive neurons; green, S100A10-positive astrocytes

FIGURE S4 Representative confocal images of dual immunofluorescence staining of S100A10 and NeuN in CA4/DG regions of cognitively normal and AD donors. Red, NeuN-positive neurons; green, S100A10-positive astrocytes. S100A10-positive astrocytes engulf NeuN-positive neuron debris as shown by the arrows. Scare bar: 10 μm

FIGURE S5 Representative images of dual immunofluorescence staining of S100A10 and APP in the CA1, CA2, CA3, CA4/DG and EC regions of Pre-AD donors. Red, APP protein; green, S100A10-positive astrocytes. Scale bar: 50 μm

FIGURE S6 Representative images of dual immunofluorescence staining of S100A10 and Aβ in the CA1, CA2, CA3, CA4/DG and EC regions of Pre-AD donors. Red, Aβ peptide or plaque; green, S100A10-positive astrocytes. Scale bar: 50 μm

FIGURE S7 Expression heatmap of the total 4133 proteins identified in cognitively normal donors

FIGURE S8 Representative images of dual immunofluorescence staining of S100A10 and Aβ or GFAP and thioflavin (specific binding to Aβ) in the EC region of Pre-AD donors. Scale bar: 50 μm

Table S1 The basic information of involved donors

TABLE S2 The antiboly list used in this study

Table S3 The total proteins identified in three sets with mass spectrum

Table S4 The GO enrichment analysis of total and differential expressed proteins

Table S5 The filtered differential expressed proteins associated in AD

Table S6 The p-value calculated based on data in Figure 7C–D using One-way ANOVA followed by the Bonferroni post hoc test

How to cite this article: Gao Y, Liu J, Wang J, Liu Y, Zeng L-H, Ge W, et al. Proteomic analysis of human hippocampal subfields provides new insights into the pathogenesis of Alzheimer's disease and the role of glial cells. Brain Pathol. 2022;32:e13047. https://doi.org/10.1111/bpa.13047